

REVIEW ARTICLE OPEN

Reconfigurable systems for multifunctional electronics

Jia Zhu¹, Michael Dexheimer¹ and Huanyu Cheng^{1,2}

Reconfigurable systems complement the existing efforts of miniaturizing integrated circuits to provide a new direction for the development of future electronics. Such systems can integrate low dimensional materials and metamaterials to enable functional transformation from the deformation to changes in multiple physical properties, including mechanical, electric, optical, and thermal. Capable of overcoming the mismatch in geometries and forms between rigid electronics and soft tissues, bio-integrated electronics enabled by reconfigurable systems can provide continuous monitoring of physiological signals. The new opportunities also extend beyond to human-computer interfaces, diagnostic/therapeutic platforms, and soft robotics. In the development of these systems, biomimicry has been a long lasting inspiration for the novel yet simple designs and technological innovations. As interdisciplinary research becomes evident in such development, collaboration across scientists and physicians from diverse backgrounds would be highly encouraged to tackle grand challenges in this field.

npj Flexible Electronics (2017)1:8; doi:10.1038/s41528-017-0009-6

INTRODUCTION

Miniaturization of integrated circuits has been a long lasting pursuit for electronic devices in the past few decades. It becomes increasingly challenging owing to the quantum effect in the nanoscale, when we approach the limit of Moore's law.¹ Due to exceptional mechanical, electric, optical, and thermal properties, low dimensional materials² complement Si in providing a new platform to enable the next generation of modern technologies. These low dimensional materials can be semiconductors, insulators, metals, and even superconductors at cryogenic temperatures. Integration of these nanomaterials enables applications from flexible and self-powered electronics³ to advanced optoelectronics and photonics.⁴

To go beyond the capability of existing materials, metamaterials⁵ are explored. In comparison to crystal materials that are periodic at the atomic scale, metamaterials are periodic with a "lattice constant" in a unit cell at a much larger scale, but smaller than a corresponding wavelength. As an effective means to transport media, metamaterials can be carefully designed in geometric parameters (e.g., shape, arrangement, and orientation) to control wave propagation, including attenuation,⁶ absorption,⁷ super lens for imaging,⁸ and negative refraction and cloaking.⁹

Physical invariance in both geometry and property remains a hallmark for modern electronic devices. In a different attempt, the reconfigurable electronic systems can change geometry and multiple desired physical properties induced by deformation. Heterogeneous integration¹⁰ of multiple materials in a composite structure or collectively in a single system can exploit the merit of each material component. In particular, integration of rigid inorganic materials on soft polymers in a reconfigurable system for bio-integrated electronics¹¹ can overcome the mismatch of geometries and forms between rigid electronics and soft biological tissues. Meanwhile, functional soft materials^{12, 13} can be incorporated into the device design for control of deformation from various external stimuli, such as electric signal, hydration, pH,

temperature, and light. In addition, actuators that are based on functional soft materials have important applications in drug delivery, artificial muscles, and soft robotics.

In this mini review, we will first briefly review the intrinsically stretchable materials and the strategies that enable stretchable characteristics to intrinsically brittle materials for reconfigurable structures in Section 2. Next, we will discuss deformable low dimensional materials in Section 3. The application of stretchable materials and structures in metamaterials with characteristic frequency regimes from acoustic and electromagnetic to photonic will then be introduced in Section 4. In Section 5, we will highlight a few representative examples from both discrete components and integrated systems in functional devices. Finally, future perspectives and conclusions will be provided in Section 6.

STRETCHABLE MATERIALS AND RECONFIGURABLE STRUCTURES

Stretchable materials¹⁴ and reconfigurable structures¹¹ represent two separate types of strategies to induce changes in configuration. Extensive reviews have been provided for both stretchable materials^{14, 15} and reconfigurable structures.^{11, 16} Therefore, only a brief review of highlights from these reviews will be discussed in this section.

Stretchable materials

Intrinsically soft and stretchable, most organic materials can deform directly upon mechanical loading or other environmental cues. Due to advantages in easy preparation, a wide range of Young's moduli, and good adhesion, silicone-based organic polymers are widely used as stretchable and reconfigurable materials. Responsive hydrogels¹² have begun to gain attention, due to their responses to various environmental stimuli, including temperature, light, and pH value (Fig. 1a). Electro-active polymers that are actuated by ion diffusion (e.g., ionic polymer) or electric

¹Department of Engineering Science and Mechanics, The Pennsylvania State University, University Park, Pennsylvania 16802, USA and ²Materials Research Institute, The Pennsylvania State University, University Park, Pennsylvania 16802, USA
Correspondence: Huanyu Cheng (huanyu.cheng@psu.edu)

Received: 2 January 2017 Revised: 16 March 2017 Accepted: 30 March 2017

Published online: 02 November 2017

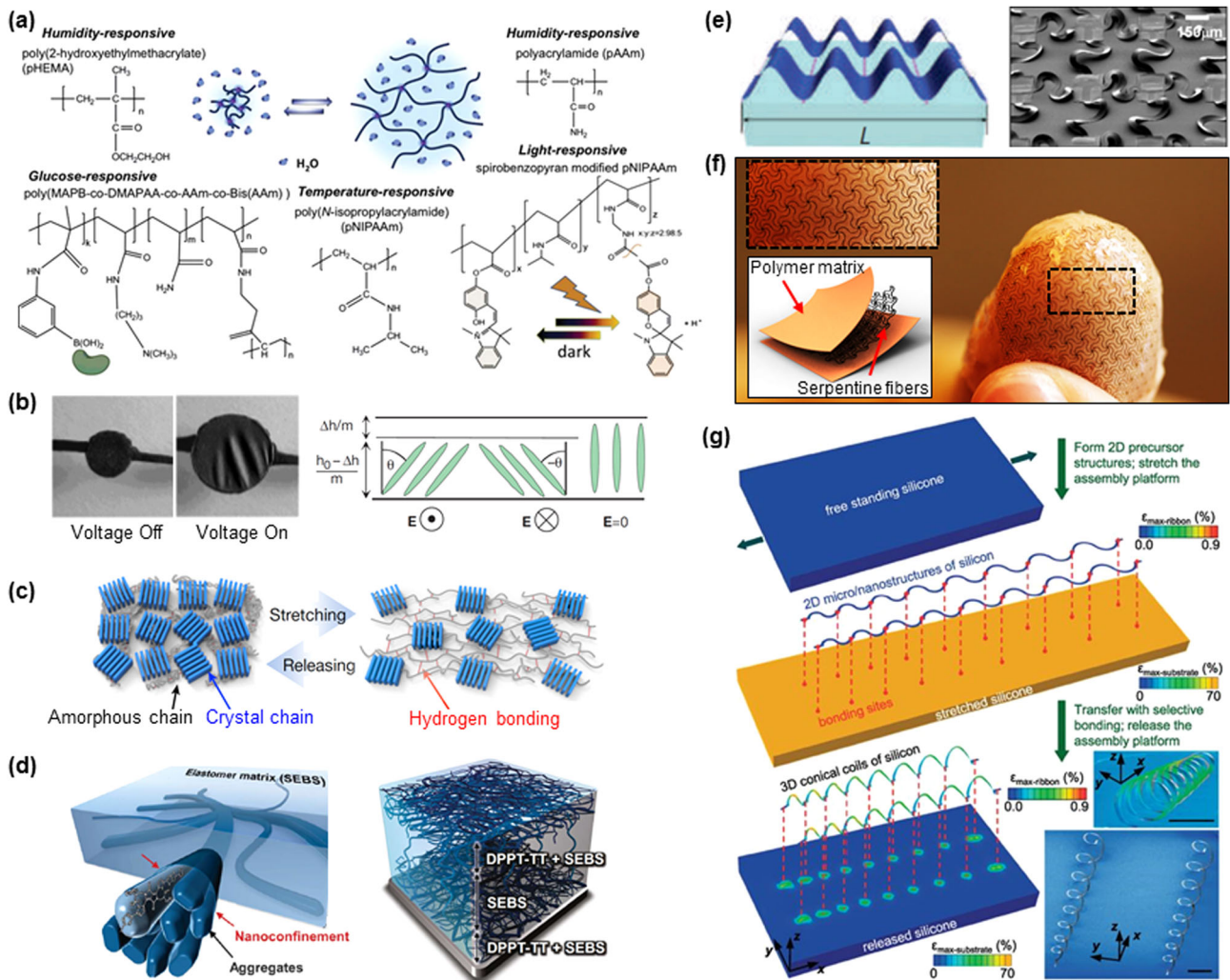


Fig. 1 Stretchable materials and reconfigurable structures. **a** A variety of hydrogels responsive to different stimuli that include humidity, temperature, light, and glucose. Reprinted with permission from ref. 12. **b** Electrostatic attraction between electrodes generates an electrostatic pressure on the film of dielectric elastomer, leading to a contraction in the thickness and an expansion in area. Electrically activated liquid-crystal elastomers lose the nematic order and relax to their coiled conformation, resulting in a thickness reduction. Reprinted with permissions from refs. 17 and 18. **c** Introducing non-conjugated moieties directly in the polymer backbone as hydrogen-bonding units enhances stretchability in conjugated polymers, due to the effective energy dissipation through breakage of bonds. Almost full recovery of the carrier mobility has been demonstrated after the solvent and thermal healing treatment. Reprinted with permissions from ref. 19. **d** Embedding nanoscale networks of semiconducting polymer achieves high stretchability from a reduced modulus and delayed onset crack propagation. Both the decreased glass transition temperature and suppressing crystallization contributed to the reduced modulus. Additional layer of soft elastomer sandwiched between two composite layers with nanoconfinement further suppresses crystallization and prevents crack propagation. Reprinted with permissions from ref. 20. **e** Selected bonding of thin ribbons to a pre-stretched substrate, followed by a release of the pre-strain, results in a wavy geometry in the thin ribbon (left). Functional components that are connected by wavy metallic interconnects in an “island-bridge” layout on a soft polymer are capable of deforming into an arbitrary shape (right). Reprinted with permission from refs. 22 and 24. **f** Schematic illustration of an artificial skin construct that exploits a two-dimensional network of photolithographically defined polyimide filaments embedded in the middle of a soft polymer matrix. Adapted with permission from ref. 28. **g** Mechanical assembly of 3D single-crystal Si conical helices from 2D filamentary serpentine ribbons bonded at selected points (red dots) to a pre-stretched silicone elastomer. Release of the pre-stretch results in an out-of-plane motion in the Si ribbon to form 3D structures. Lower right shows SEM images of an experiment. Reprinted with permission from ref. 30

fields (e.g., dielectric elastomer,¹⁷ liquid-crystal elastomer¹⁸) also appear as emerging feasible materials to mimic muscle movements¹³ (Fig. 1b). Intrinsically stretchable semiconducting polymers are of particular interest, due to their essential role in thin-film field-effect transistors (FETs). Introducing hydrogen bonding between amorphous chains of flexible polymer effectively dissipates energy for an applied strain, while maintaining high carrier mobility and almost full recovery after a solvent and thermal healing treatment¹⁹ (Fig. 1c). Alternatively, nanoconfinement has also been explored to substantially increase the stretchability of semiconducting polymers, by reducing the

modulus and delaying the onset crack formation²⁰ (Fig. 1d). Similarly, loading carbon nanotubes (CNTs) in the soft polymers provide a highly conductive pathway for charge transport.²¹ In addition to CNTs-based stretchable conductors, their metallic nanomaterial counterparts¹⁵ such as 1D nanowires and 0D nanoparticles can also be dispersed in the polymer matrix for high conductance. These stretchable materials are also exploited as substrates in reconfigurable structures (see Section 2.2), to transfer and trigger the deformation in those structures.

Reconfigurable structures

In a different direction to soft, organic materials, several strategies in reconfigurable structures enable stretchable properties to intrinsically brittle inorganic materials. The idea of spring behind wavy structures is one simply yet effective means. The concept in the strategy of pre-strain first laminates a film onto a pre-stretched soft elastomer and then the release of this pre-stretch induces forces to deform the film into a wavy structure in the out-of-plane direction^{22, 23} (Fig. 1e, left). The other similar but more versatile strategy exploits an initially wavy geometry of metallic interconnects between active device components in the in-plane surface. When the thickness of interconnects is much smaller than their width, wavy interconnects would deform out-of-plane upon stretching. Connecting functional components with this type of wavy metallic ribbon in an array, often termed as “island-bridge” layout^{24, 25} (Fig. 1e, right), provides a stretchable form for the device system. Integrating such a device layout on a soft substrate in a way that only functional components are fully bonded to the structured substrate²⁶ further isolates the deformation²⁷ to the regions of wavy metals. In the application of bio-integrated electronics, it is desirable to match the effective modulus of devices to that of the skin even for various levels of stretching. In order to address this challenge, composite structures that embed serpentine fibers in a polymer matrix to mimic the living fabric in the biological tissues has also been explored in the substrate^{28, 29} (Fig. 1f). In a separate but related approach to reconfigure structures, the idea of origami has also been explored to transform a pre-patterned 2D geometry into a 3D structure³⁰ (Fig. 1g). This method can overcome the limitation of lithography and 3D printing to construct 3D structures from advanced materials, particularly semiconductors.

DEFORMABLE LOW-DIMENSIONAL MATERIALS

Taking Si as the DNA of our technology evolution, advent of low dimensional materials provides mutation to the genes of modern electronics, as they possess combined outstanding mechanical and electric properties. Exploiting mechanical mismatch between low dimensional nanomaterials and polymeric substrates can

trigger desired structural instabilities in low dimensional nanomaterials. Such techniques of strain engineering provides an effective means to tune the electronic property in low dimensional materials.³¹

1D nanomaterials

With a lateral dimension in the nanoscale, 1D nanomaterials,¹⁵ in the forms of ribbons, belts, wires, and tubes, demonstrate outstanding mechanical property and interesting electronic, optoelectronic, and thermal properties, enabling applications in mechanical sensing/actuation and energy harvesting. These 1D nanomaterials can be fabricated by anisotropic growth from templates or crystallographic structures. Piezoelectric nanowires and CNTs represent two of the most widely applicable forms of deformable nanomaterials, for their lightweight and low power consumption. Exhibiting a wide array of physical properties, these nanowires are utilized across many fields, with applications from tunable electronic structures that use the piezoelectric effect to flexible electrodes.

Among the currently existing 1D nanomaterials, zinc oxide (ZnO) is sought after for its semiconducting and piezoelectric properties. Formation of the Schottky barrier between the metal tip and ZnO nanowire can be utilized to construct electricity-generating devices for energy harvesting from deformation, when integrated on soft substrates. This electricity-generating technique has the potential to convert various forms of mechanical energy (e.g., biological mechanical, acoustic/ultrasonic vibration, and bio-fluid hydraulic energies) into electrical energy, theorizing new ways to power various nanodevices. In one demonstration, a single ZnO nanowire is fixed to an intrinsic silicon substrate for its low conductivity.³² When a force of 5 nN is applied between the tip of an atomic force microscope and sample surface, the mechanical manipulation of the wire generates an output voltage of -5 mV. Only when the tip passes over the wire is there an observed output voltage, with no external voltage being applied to the system (Fig. 2a).

Conducting or semiconducting CNTs can form in controlled density, spatial distribution, length, and orientation. Prepared on thermally stable substrates, horizontally aligned, vertically aligned,

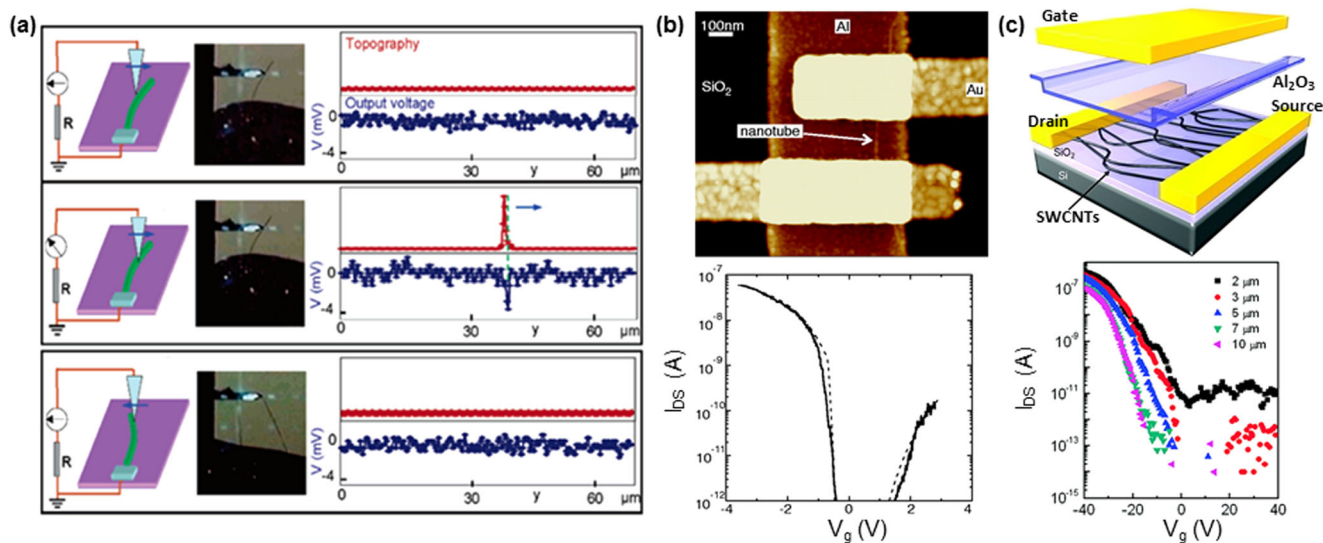


Fig. 2 Deformable 1D materials. **a** Schematic demonstration of the working principle of nanogenerators that are based on a single ZnO nanowire. The simultaneously recorded topography and electric response of the system indicate the piezoelectric current only forms when the AFM probe goes over the nanowire from one side to the other. Reprinted with permission from ref. 32. Field effect transistors (FETs) with **b** a single semiconducting carbon nanotube (CNT) or **c** a CNTs network as active channels. The lower panel shows the experimentally measured drain current as a function of gate voltage for a constant drain-source voltage of 5 mV (**b**: a single CNT) and 100 mV (**c**: a CNTs network for different channel lengths), respectively. FETs with a CNTs network active channel exhibit enhanced on/off ratio for an increased semiconducting channel length. **b** and **c**: Reprinted with permissions from refs. 35 and 38, respectively

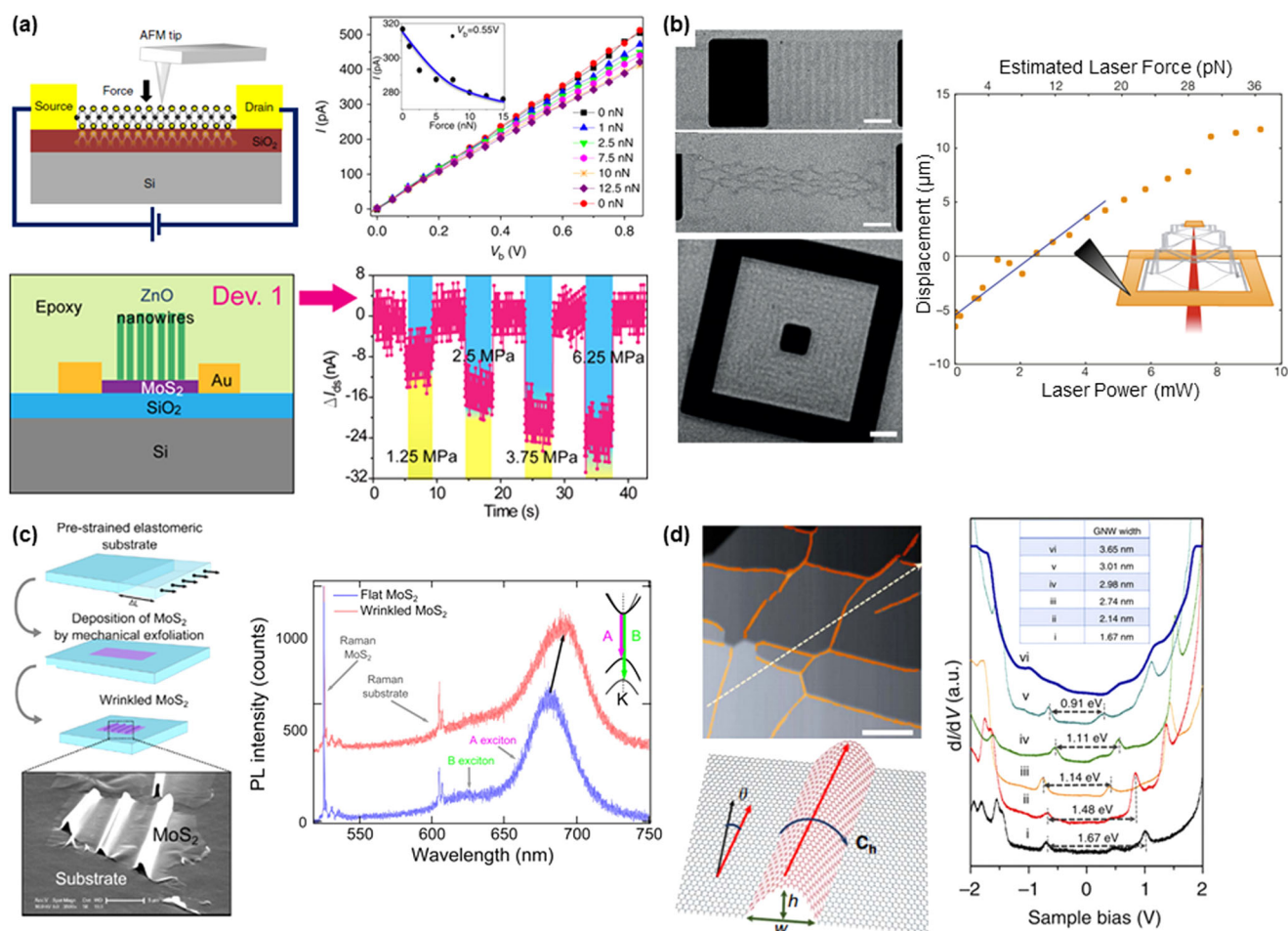


Fig. 3 Deformable 2D materials. **a** Schematic of FETs that are based on a MoS₂ monolayer (upper left) or a ZnO nanowire and MoS₂ monolayer hybrid structure (lower left). The right panel shows the mechanical tunable characteristics of the corresponding FETs. Reprinted with permissions from refs. 43 and 44. **b** Graphene kirigami in the shapes of microscale springs (upper left) and pyramids (lower left) for enhanced stretchability and deformability. Actuated by lasers, a force–distance curve for a pyramid can be obtained, from which a linear fit at low forces yields a spring constant of $2 \times 10^{-6} \text{ N m}^{-1}$ (right). Reprinted with permission from ref. 46. **c** Experimental steps to obtain rippled MoS₂ with an AFM image shown at the bottom (left). Photoluminescence emission measurement from the flat (blue) and wrinkled (red) regions in the same MoS₂ flake shows a red shift in a wrinkled region, indicating a reduced band gap due to the local strain (right). Adapted with permission from ref. 31. **d** Recolored AFM image of epitaxial graphene grown on Ni (111) by a rapid cooling process, with wrinkles highlighted in orange (left, schematic drawing of the wrinkle at the bottom). dI/dV spectra obtained from graphene nanowrinkle (GNW) with different widths by scanning tunneling microscopy. The band gap marked by double dashed arrows decreases as the wrinkle width increases, due to reduced local strain. Reprinted with permission from ref. 49

or network-like CNTs can be transferred onto soft substrates via the technique of transfer printing.^{33, 34} When doping is used to reduce the sheet resistance, the conducting CNTs in a high density can be used as electrodes. In comparison to conventional electrodes, CNTs-based conducting films are stretchable, enabling applications in soft displays and bio-integrated devices. In addition, semiconducting CNTs have been exploited as active channels in FETs for lightweight and low power consumption devices. With a single CNT as active channel³⁵ (Fig. 2b), FETs have shown large on/off ratios, but poor carrier mobility, which can be improved by employing aligned CNTs³⁶ or random CNTs network^{37, 38} (Fig. 2c).

2D materials

There has been an increasing interest in 2D nanomaterials, due to their unique mechanical, electrical, magnetic, optical, and thermal properties, which are not found in their bulk counterparts. In particular, successful experimental realization of 2D monolayer conducting (e.g., graphene) and semiconducting (e.g., hexagonal boron–nitride and transit metal–dichalcogenides) materials

presents new opportunities for electronics. These 2D nanomaterials are typically associated with a very large Young's modulus (e.g., $Y_{\text{graphene}} \sim 1.0 \text{ TPa}$,³⁹ $Y_{\text{MoS}_2} \sim 270 \text{ GPa}$ ⁴⁰) due to the close-packed hexagonal lattice and interatomic covalent bonding. However, the small thickness allows these 2D nanomaterials to bend over a small radius of curvature such as several nanometers for monolayer MoS₂⁴¹ and to sustain moderate stretching (e.g., >20 % stretching for graphene⁴² and 11% for MoS₂⁴⁰).

The 2D conducting and semiconducting nanomaterials that are exploited in FETs demonstrate low power consumption due to a high carrier mobility.^{43, 44} Due to the good Schottky contact, the FETs with MoS₂ as transistor channels (Fig. 3a, top) are reported to have large on/off ratio and strain-tunable drain current, known as the piezoresistive effect.⁴³ This tunable property results from a change in the built-in field along the channel from the piezoelectric charge, which in turn changes the Schottky barrier height between two contacts.⁴³ By stacking 1D ZnO nanowire array on top of 2D MoS₂ channels (Fig. 3a, bottom), drain current or IV curve of FETs can be tuned by applied pressure, in a high sensitivity with potential applications for electronic skin.⁴⁴ The high sensitivity is

attributed to the change of MoS₂ band structure from the strain-induced piezoelectric polarization charges at the 2D/1D interface.

As another popular 2D material, graphene is usually used as electrodes in FETs due to its zero band gap. However, the band gap of graphene opens up upon applied strain, which turns it from a conductor to semiconductor, enabling graphene channels in FETs. In comparison to chemical doping/modification or external electric field, strain engineering can easily control the change of band gap.⁴⁵ Considering the high carrier mobility, graphene can be a very promising alternative for Si in the electronics industry. Relative motion within the same graphene monolayer engineered by the concept of kirigami on a micrometer scale opens up the opportunities to apply 2D nanomaterials to storage, micro robots, and medical delivery⁴⁶ (Fig. 3b). For example, with designed hydrogenated edges, a graphene origami can form 3D structures through hydrogenation by a trigger in the electric field for potential hydrogen storage.⁴⁷ In another example, a four-legged walking robot that is based on single graphene oxide film with asymmetric surfaces can move forward even on smooth glass substrate step by step, by alternating the infrared light on and off.⁴⁸

Structural instabilities (e.g., buckling, ripples, and wrinkles) of 2D nanomaterials lead to change in electronic structures. The

structural instabilities such as ripples and wrinkling have been demonstrated in the experiment to modify the intrinsic mechanical properties of 2D nanomaterials. As one representative example, periodic MoS₂ ripples can form through the strategy of pre-strain with a uniaxial pre-strain of 100%³¹ (Fig. 3c). With selective delamination from the substrate, the MoS₂ layer forms sinusoidal ripples. Thicker MoS₂ flakes correspond to larger amplitude and wavelength in the ripples. Both the Raman and photoluminescence spectra of the rippled region show peak shifts, whereas there is none in the flat region, verifying the change of band structures of MoS₂ induced by the local strain.³¹ However, the reason for selective delamination of MoS₂ from the substrate still remains unclear. Elucidating such mechanism will surely help the design of local strain engineering for engineered electrical properties. Due to the large mismatch in coefficients of thermal expansion, nanowrinkles can also form at the graphene/Ni interface by growing graphene on a Ni (111) substrate followed by a rapid cooling process (Fig. 3d). Scanning tunneling microscopy reveals that the band gap of graphene is opened in the delaminated region. The inverse proportional dependence of band gaps on the width of wrinkles indicates that the opening of band gap originates from the 1D confinement of electrons.⁴⁹

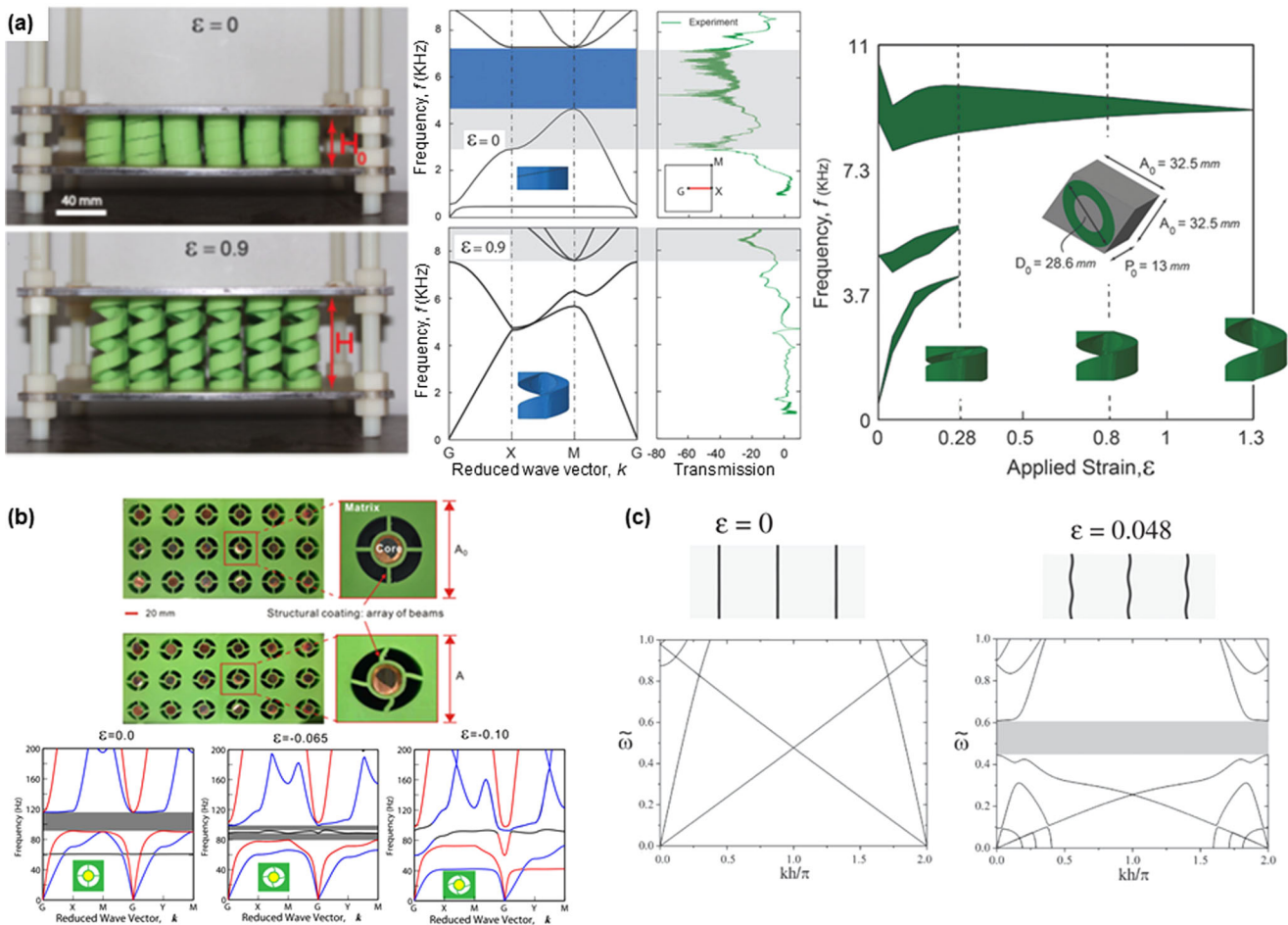


Fig. 4 Acoustic metamaterials. **a** Optical images of the initial and deformed acoustic metamaterials composed of an array of 6 by 6 stretchable helices (upper left). When the array is arranged in a square lattice, calculated band structures of the initial and deformed metamaterials show a stretching of 0.9 leads to the switch-off of the band gap (marked by the blue region) (left). The right shows the evolution of the band gap for a triangular array (a stretching of 1.3 for close-up of the band gap). Adapted with permission from ref. 57. **b** Each resonator consists of a metallic mass core connected to the matrix through four elastic beams, where black regions indicate voids in the structure (top). When a compressive strain of 0.10 is applied in the vertical direction, buckling of the vertical beams alters the effective stiffness of the structure. The band structure is split and eventually turned off for an increasing compression. Reprinted with permission from ref. 58. **c** Due to a mechanical mismatch between adjacent layers, interfacial buckling in a periodic multilayered structure opens up a band gap. Reprinted with permission from ref. 59

DEFORMABLE METAMATERIALS

When the lattice constant is much smaller than the wavelength, the metamaterial can be treated as a homogeneous transport media with effective parameters that are the average in a single unit cell. This leads to the exploration of negative index materials for cloaking and super lensing. However, when the lattice constant is relatively large, the Bloch theorem, rather than the effective media model, has to be applied to help understand the wave propagation, such as attenuation characterized by the band gap. As dictated by the Bloch theorem, waves in periodic structures take on the same symmetry and periodicity of their host materials/structures. As the geometry of the metamaterial plays a critical role in determining the aforementioned properties, reconfiguration of metamaterials⁵⁰ has been explored through deformation introduced by external stimuli.⁵¹ According to the length scale, metamaterials can be categorized into acoustic, electromagnetic, and photonic regimes. The acoustic wave is governed by the frequency domain Helmholtz equation, whereas the other two are governed by the Maxwell equations. In the following, we will briefly review these three types of metamaterials according to their regimes of functional frequency.

Acoustic metamaterials

Composed of periodic structure immersed in the air or fluid, acoustic metamaterials are designed to manipulate the propagation of sound waves. The geometry of such structure can be used to tune the band gap in the dispersion curve. For example, a hypersonic band gap can be created in face-centred-cubic colloidal crystals formed by self-assembled polystyrene nanoparticles with subsequent fluid infiltration.⁵² Increasing the particle size from 256 to 307 nm leads to a shift in the center of band gap from 4.2 to 4.8 GHz. In another example that exploits a bistable beam elements connected by elastomeric linear springs, an acoustic metamaterial can damp linear waves in dissipative polymer, but propagate a stable, nonlinear solitary transition waves, with high fidelity and controllability for signal control.⁵³ The band gap can be effectively modulated through local resonance in a unit cell, which can be used to design acoustic composites with negative densities and moduli by suspending soft rubber spheres in water.⁵⁴ Building on this concept, unique acoustic properties such as cloaking⁵⁵ and super lens for imaging⁵⁶ have been demonstrated as well.

As geometry of metamaterials plays a critical role in determining their band structure (such as on/off and position of a band

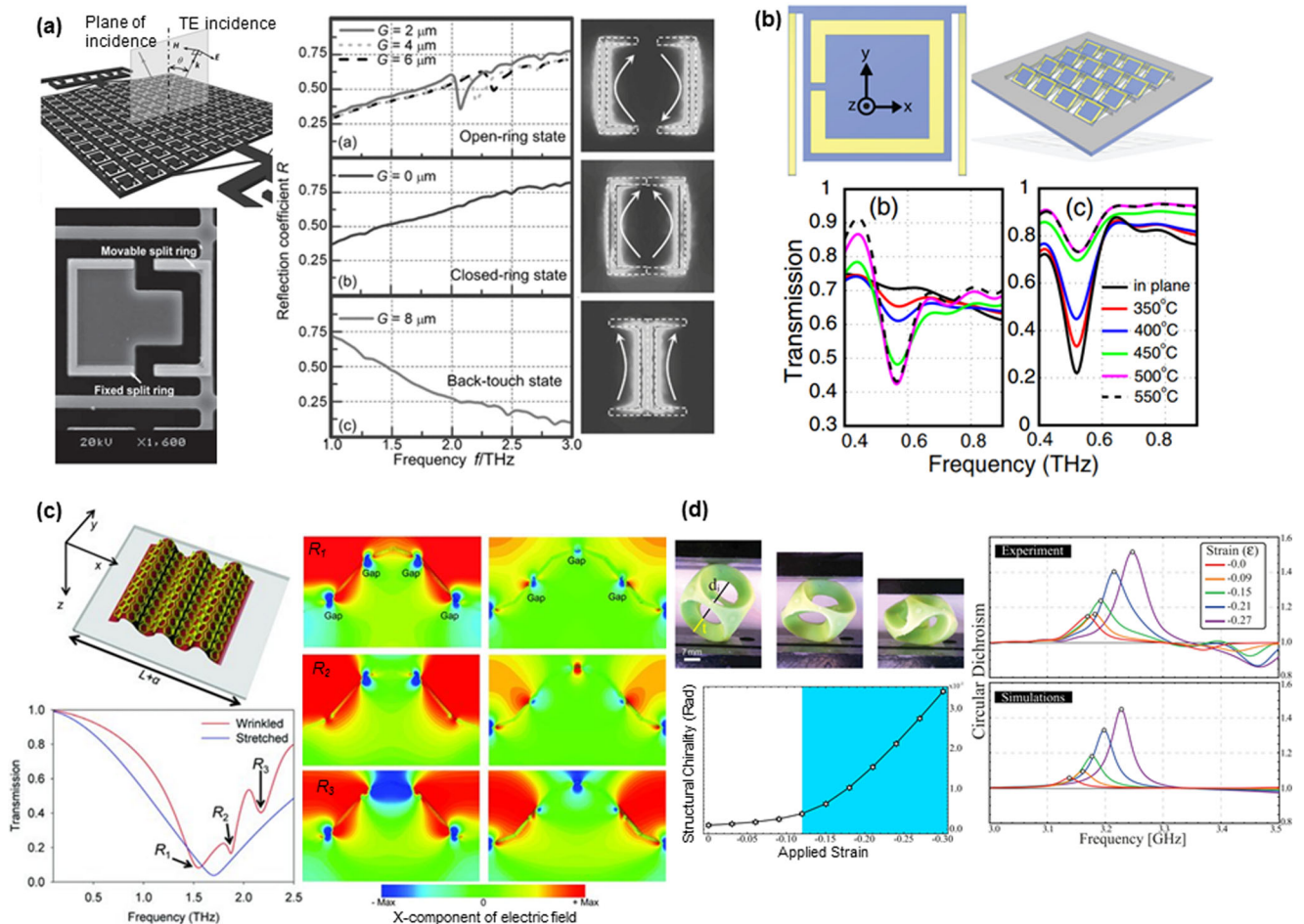


Fig. 5 Electromagnetic metamaterials. **a** Switchable magnetic metamaterial capable of changing the gap between two split rings by an actuator through Coulombic force (left, a magnified unit cell shown at the bottom). The right shows measured reflection coefficients of the metamaterial with different gaps. Reprinted with permission from ref. 61. **b** Reconfigurable metamaterials that can change the orientation of split rings through bending of cantilever legs, triggered by temperature change. The lower panel demonstrates the magnetic and electric responses of this reconfigurable metamaterial for various temperatures. Reprinted with permission from ref. 51. **c** Honeycomb-shaped metamaterial forms a wavy surface by the strategy of the pre-strain. Three different resonance modes resulting from the wavy geometry are demonstrated by the three different dips in the transmission spectrum (right). Reprinted with permission from ref. 62. **d** Structural chirality increases with compression in a buckleball-shaped metamaterial with metallic insertion. Experimental measurements and simulation of circular dichroism as a functional of increasing compression strains are shown in the right. Reprinted with permission from ref. 63

gap), introducing soft, reconfigurable materials in acoustic metamaterials provides dynamic control of the acoustic band structure. As shown in Fig. 4a, an array of elastomeric helices manufactured from a molding and casting method can reconfigure its pitch and diameter in an approximately linear manner upon external loading.⁵⁷ The solid fraction in such structure decreases with applied tensile strain. For a square array, an acoustic band gap in its undeformed configuration disappears when the stretching reaches 0.9. The stretching to close the band gap changes to 1.3 for a triangular array. In addition to the arrangement of unit cells, the band gap frequencies also depend on cross sectional dimensions and geometry of unit cells. Similarly, in-plane buckling of four evenly spaced beams that connect the inner metal cores and the matrix changes the effective stiffness of the structure, which leads to the shift of resonance frequency⁵⁸

(Fig. 4b). Under compression, the acoustic band gap decreases and further splits due to softening of two beams in the compression direction and the rotation mode, and eventually closes because of the modal transformation of the rotational band near the G point. In another example that utilizes buckling to form sinusoidal interface upon uniaxial compression in layered structures, the acoustic band structure can effectively evolve for a different combination of material properties, geometries and incident angles⁵⁹ (Fig. 4c).

Electromagnetic metamaterials

Electromagnetic metamaterials use negative permittivity and/or permeability to enable tailoring of electric and magnetic response⁶⁰ of the material. By exploiting the LC circuit, negative

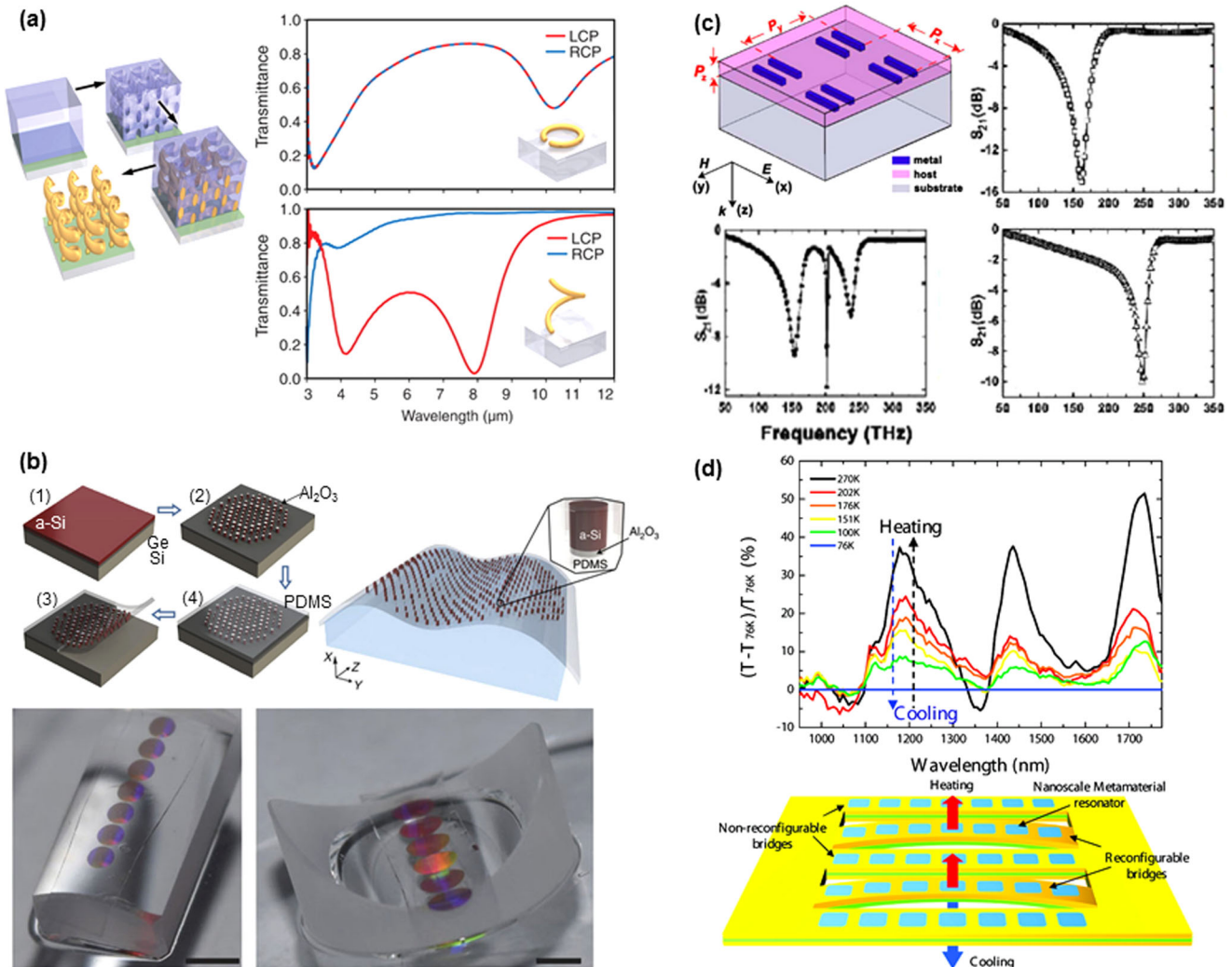


Fig. 6 Photonic metamaterials. **a** Fabrication process to form an array of air helices through 3D direct laser writing of polymer, gold plating, and removal of the polymer (left). The right shows 2 by 2 mm unit cells with 2 mm helix pitch used in the calculations and normal incidence transmittance spectra for light impinging from the air side (RCP and LCP: right and left-handed circular polarization of the incident light). Right part demonstrates that the transformation from 2D to 3D structure leads to the selection on the polarization of light propagating through it. Adapted with permission from ref. 65. **b** Amorphous silicon nano-posts on a thin layer of aluminum oxide embedded in a low-index flexible substrate as a metasurface can conform to surfaces of arbitrary shape. Either a convex (lower left) or a concave (lower right) glass cylinder coated with a metasurface can behave as an aspherical lens to focus light to a point. Adapted with permission from ref. 66. **c** In a metamaterial composed of metallic double bars, transmission spectrum only shows one resonance mode, when the double bars are symmetric in length (both are 120 or 200 nm, middle). Asymmetric design in double bars (120 nm for one and 200 nm for the other one) results in a new resonance mode due the coupling of LSPR. Reprinted with permission from ref. 69. **d** A thermally tunable metamaterial structure consisting of alternating reconfigurable and non-reconfigurable bimaterial bridges shows temperature tunable transmission normalized to a reference temperature of 76 K. Bilyered beam in reconfigurable bridges will bend in response to temperature changes, whereas no bending for a symmetric layer layout in non-reconfigurable bridges (right). Reprinted with permission from ref. 72

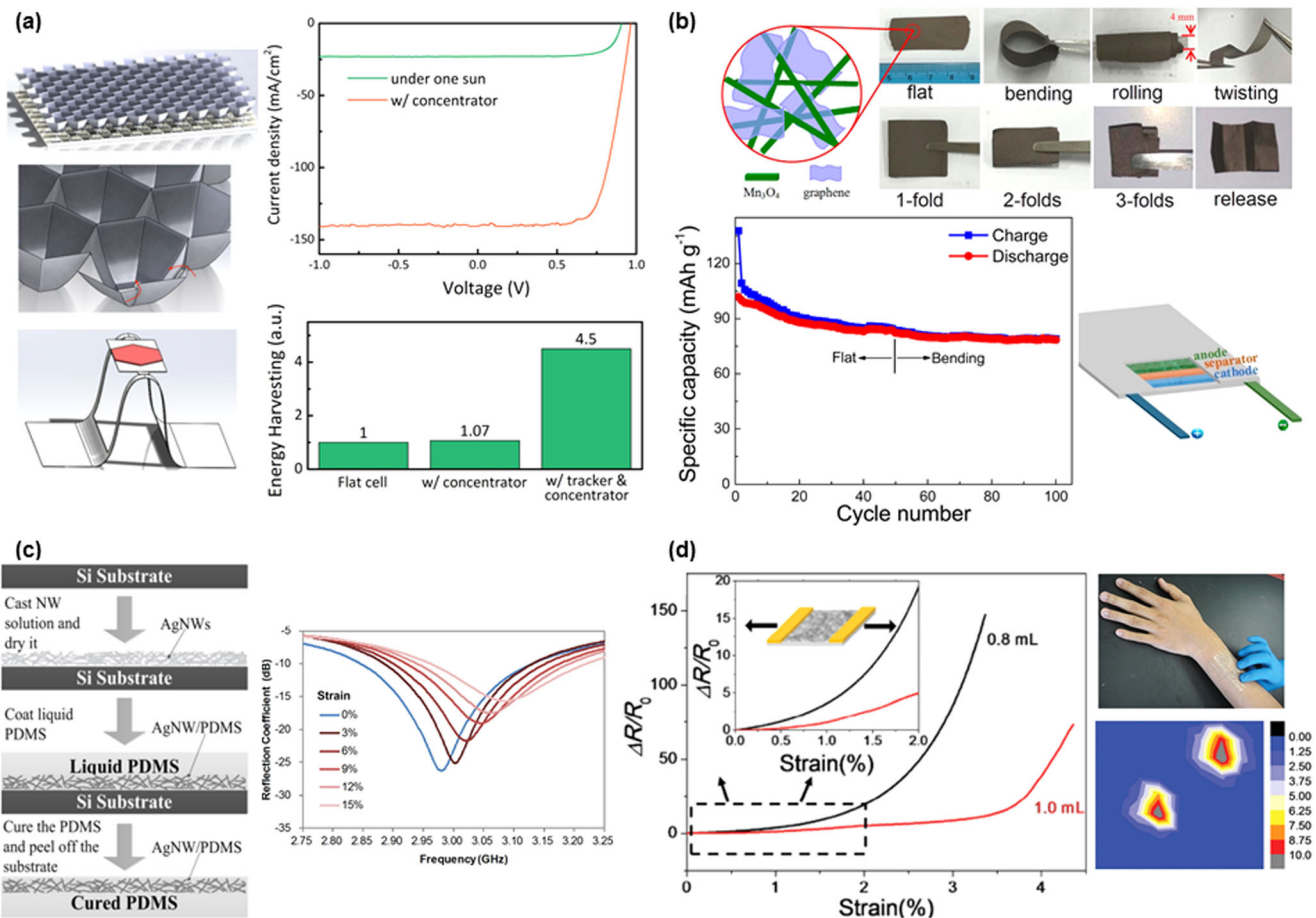


Fig. 7 Discrete components. **a** Solar cells with origami concentrators (lower left) and trackers (lower right) show significant improvements in diurnal energy output and light harvesting efficiency. Reprinted with permission from ref. 73. **b** (Top) digital photos of the rGO/Mn₃O₄ membrane in various deformation states (bending, rolling, twisting, and 1, 2, 3-fold; rGO, reduced graphene oxide). (Bottom) cycling performance of a flexible rGO/Mn₃O₄/LiMn₂O₄ full battery, with 3D schematic configuration shown on the right. Reprinted with permission from ref. 76. **c** Screen-printed silver nanowires embedded in the surface layer of a soft PDMS substrate form highly conductive and stretchable material for mechanically tunable patch antennas with an increased resonance frequency for an increasing stretching. Reprinted with permission from ref. 80. **d** Sliding between adjacent graphene flakes changes the graphene connection channel and its tunneling effect. The high resistance change from such sliding is exploited for wearable strain sensors to map pressures applied from two fingertips on the forearm. Reprinted with permission from ref. 81

artificial magnetism can be demonstrated through split ring resonance. Configuration of metamaterials can be controlled through the change in external fields. For example, the spacing between two semi-square split rings in a unit cell can be precisely adjusted by fixing one ring on the substrate and translating the other one by an actuator through Coulombic force⁶¹ (Fig. 5a). Such precise control in spacing effectively changes the electromagnetic reflection of this structure, leading to a *blue* shift in the resonance frequency and a decrease in the resonance strength for a decreasing gap between two adjacent split rings. By further decreasing this spacing, the structure evolves into a back-to-back configuration and the resonance completely disappears.

In addition to electrostatic force, other multi-physical fields (e.g., temperature and light) can also introduce change of geometry such as lattice constant and orientation in metamaterials. In another example that explores split Au rings and cantilever legs for terahertz metamaterials, the cantilever legs attached to a temperature responsive substrate can bend out-of-plane and reorient unit cells for a tunable electric and magnetic response, in response to a thermal stimulus⁵¹ (Fig. 5b).

Direct mechanical deformation can also be exploited to tune the electromagnetic response of metamaterials. Arrays of metallic honeycomb-shaped frames can form a wavy surface through the

pre-stretch strategy (Fig. 5c). With a change in both the orientation and geometry in each honeycomb, the transmission curve shows that buckling leads to three additional split resonant modes, in comparison to a flat geometry.⁶² Different geometries such as a patterned spherical shell with six circular holes and metallic insertion in a shape of bucklball are also demonstrated (Fig. 5d). The bucklball undergoes structural instability induced by axial compression, leading to an increased structural chirality and circular dichroism as compression increases.⁶³

Photonic metamaterials

Photonic metamaterials start to gain increasing attention due to their potential applications in bio-imaging and bio-sensing. Photonic or plasmonic metamaterials/metasurfaces can exhibit desired transmission and reflection spectra, because of the strong coupling between photons and electrons.⁶⁴ In addition to transmission and reflection, modulation of chirality results in the change of the polarization of light. Three-dimensional gold helices arranged in a two-dimensional square lattice are capable of blocking circular polarized light with the same handedness as the helices while transmitting the others, over a relatively large frequency range (Fig. 6a). In addition to the common building blocks of metal nanoparticles or nanorods, the dielectric materials

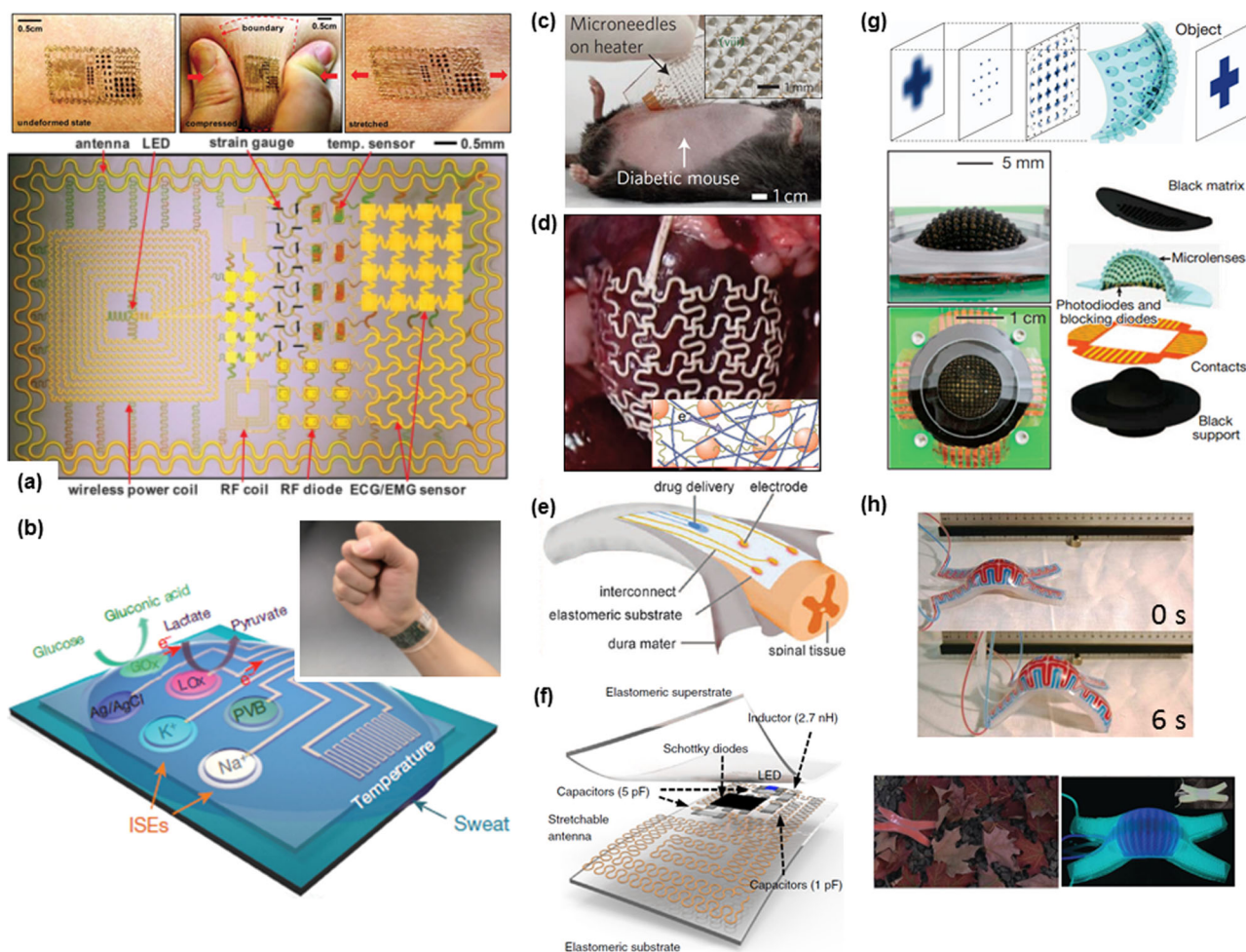


Fig. 8 Integrated systems. **a** Integrating multiple functional components that include sensors, LEDs, wireless data/power modules in a single epidermal platform enables such electronics to continuously transmit the monitored physiological signals to the external circuits. Reprinted with permission from ref. 90. **b** Fully integrated wearable sensor array for real-time perspiration analysis, including metabolites (e.g., glucose and lactate) and electrolytes (e.g., sodium and potassium ions). Reprinted with permission from ref. 91. **c** Optical image of the gold-doped graphene heater integrated with the drug-loaded microneedles (inset) on the skin near the abdomen of the mouse with hair shaved off. The dissolution of a thermally active bioresorbable coating layer on microneedles triggers transdermal delivery of Metformin to reduce blood glucose levels. Reprinted with permission from ref. 92. **d** Photograph of the epicardial mesh implanted on heart, where the mesh was fabricated by dispersing conductive Ag nanowires (AgNW) homogeneously in the organic-phase styrene-butadiene-styrene (SBS) rubber network. Inset shows stretched elasto-conductive mesh (ball: hard domain in SBS, wavy yellow line: elastic domain in SBS, straight blue line: conductive nanowire with polyvinylpyrrolidone ligand of AgNW partially exchanged to hexylamine using NOBF₄). Reprinted with permission from ref. 93. **e** Schematic illustration of the electronic dura mater inserted in the spinal subdural space of rats for electrical excitation transmission and local drugs delivery. Reprinted with permission from ref. 95. **f** Exploded view schematic of the optoelectronic system with an integrated LED and an energy harvester component to wirelessly modulate neuronal activity. Reprinted with permission from ref. 96. **g** Arthropod-inspired cameras on hemispherical shapes with a wide-angle field of view, low aberrations, high acuity to motion, and an infinite depth of field. Exploded view illustrates the components of this system: perforated sheet of black silicone (black matrix), hemispherical array of microlenses and photodiodes/blocking diodes, thin film contacts for external interconnects, and hemispherical supporting substrate of black silicone. Reprinted with permission from ref. 97. **h** A soft quadruped moves through actuation from microfluidic channels (left, major ruler division of 1 cm). The microfluidic network also enables camouflage (upper right) and display coloration (lower right, glowing in the dark using chemiluminescence; inset, the same robot photographed in the light). Reprinted with permission from ref. 100

have also been exploited for photonic metamaterials, due to their low loss.⁶⁵ Due to a thin geometry of the metasurface with a building block of cylindrical amorphous silicon nano-posts on a thin layer of Al₂O₃ embedded in a low-index flexible polydimethylsiloxane (PDMS) substrate (Fig. 6b), the metasurface can conform to a non-planar arbitrarily shaped geometry without change of resonance frequency. In such metasurface, optical function can be decoupled from geometrical form. As a proof of concept, a convex glass cylinder covered by a metasurface can function as an aspherical lens to focus light to a point.⁶⁶

When the frequency enters the light regime, the scaling law that the resonant frequency scales inversely with the characteristic

dimension of the structure breaks down, because the kinetic energy and inertia of electron cannot be neglected as those in low frequency regimes. The localized surface plasmon resonance (LSPR) in each unit cell and the interaction of LSPR between cells affect resonance and thus the absorption of light, as thoroughly discussed in several review papers.^{67, 68} The interaction of LSPR between cells is complicated, but it can be understood by the electronic or molecular energy theory that indicates split in the resonance modes is due to the interaction. The damping between LSPR results in the split in resonance modes, which has been verified by the transmission curve in the experiment⁶⁹ (Fig. 6c). The orientation and geometry determine the LSPR mode, whereas

the distance between unit cells determines the coupling strength between LSPR.⁷⁰

A flexible photonic metamaterial can be obtained by coating a nano-gating structure with Au particles immersed colloids through interference lithography.⁷¹ The increasing in the grating period for a 5% stretching leads to an obvious red shift from 550 nm to 600 nm in the optical transmission.⁷¹ Spatial variation in temperature can trigger non-uniform deformation in an asymmetric structure at the interface due to the mismatch in coefficients of thermal expansion. Consisting of a 1D array of alternating reconfigurable and nonreconfigurable biomaterial bridges, reconfigurable bridges in a bilayered geometry bend in response to temperature changes, leading to increased transmission for an increased temperature⁷² (Fig. 6d).

FUNCTIONAL DEVICES

The application of bio-integrated devices is severely limited by the huge differences in mechanical properties and forms between curvy, soft tissues and planar, rigid inorganic materials for high-performance electronics. Capable of overcoming the mismatch, bio-integrated electronics can continuously monitor physiological signals. Heterogeneous integration of the reconfigurable low dimensional materials and metamaterials further opens up new opportunities for applications that include in-vivo clinical diagnostics/therapeutics and soft robotics among many more.

Discrete components

Taking advantage of the nanofabrication foundry technology, bio-integrated electronics are demonstrated with characteristic size ranging from nanometers to centimeters. Demonstrated functional components include sensors, optical lenses, power sources, and LEDs. Combined with the idea of kirigami, a planar polyethylene terephthalate glycol-modified (PETG) sheet is cut and folded into an array of solar cells, consisting of a tightly packed hexagonal concentrator and tracker. With a dynamically tunable orientation angle optimized for the incident angle of light through the folding level of PETG (Fig. 7a), the array of solar cells achieves a 450% increase in energy output.⁷³ Meanwhile, flexible solar cells that are based on transparent Ag-nanowire electrodes exhibit high power-conversion efficiency and bendability, enabling its application as a power source for flexible electronics.⁷⁴

Power source has long been a challenge for electronics, particularly for portable and wearable devices. Near-field communication⁷⁵ is simple in design, but a short transmission distance and low efficiency limit its applications. Radial frequency has the potential for long-range energy and data transmissions, but the issue of large absorption by the tissues should be addressed. Utilizing the highly conductive graphene and the high-capacity Mn_3O_4 nanowires in a nanocomposite membrane (Fig. 7b), the advanced electrode design for Li-ion battery provides enlarged electrode/electrolyte contact area and reduced electron/ion transport resistance.⁷⁶ Stretchable batteries with wireless recharging modules²⁵ have also been demonstrated, but a large footprint is still required for high output power.

As an alternative to batteries, supercapacitors possess a better cycling stability, as there is no chemical reaction involved.⁷⁷ For example, the electrochemical-sensing device that uses the MnO_2 -graphene nanohybrid paper⁷⁸ as the working electrode exhibits high specific capacitances and cycling stability, with capacitance retentions of 92% and 90% for 7000 charge/discharge cycles and 1000 times of folding/unfolding, respectively. In addition, exploiting nanoporous cellulose paper embedded with aligned carbon nanotube electrode and room temperature ionic liquid electrolyte as the basic unit, energy-storage devices⁷⁹ such as supercapacitors, Li-ion batteries, and hybrids are capable to function

over large ranges of mechanical deformation and record temperatures.

The concept of composite patch consisting of conducting nanowire network (e.g., carbon nanotubes, graphene, or Ag nanowires) can also be applied to the other functional components. In addition to energy transmission, radio frequency data communication is also indispensable in wearable tattoo electronics. For example, a flexible patch antenna with Ag nanowire embedded in a PDMS substrate matrix demonstrates strain-tunable resonance frequency, without noticeable change over stretch-and-release cycles⁸⁰ (Fig. 7c).

In contrast to the nearly unchanged property such as resistance with strain, the conductive nanomaterial networks can also be designed to have resistance extremely sensitive to the deformation. The deformation leads to relative motion such as sliding or rotation between adjacent nanostructures (e.g., nanowires, nanotubes, or nanoflakes). Such motion results in a significant change in the conducting pathway and thus conductivity of the nanomaterial network. One such example exploits the Marangoni effect at the liquid/air interface to self-assemble two layers of graphene flakes, followed by a transfer on a PDMS substrate (Fig. 7d). When the network is loosely connected, a tunneling effect between two graphene layers shows significantly increased conductivity, i.e., more than 10 times for a stretching of 2%, demonstrating the highest sensitivity thus far.⁸¹ When implemented such sensor in an array, the capability of pressure sensing opens up opportunities in electronic skin, wearable sensors, and health monitoring platforms.

Integrated systems

Integrating various modules into a single system provides a platform for continuous monitoring of health condition,⁸² augmented surgical procedures,⁸³ and human-machine interfaces.⁸⁴ A bio-integrated electronic device that includes LED,⁸⁵ antenna, and a variety of different sensors (e.g., temperature,⁸⁶ strain,⁸⁷ and electroencephalogram/electrocardiogram/electromyogram^{88, 89}) is demonstrated in a form of a soft, epidermal tattoo⁹⁰ (Fig. 8a). The data collected by the sensors can be wirelessly transferred to external data acquisition system for continuous monitoring. In addition to the physical sensors, bio-integrated chemical sensors are capable of perspiration analysis for precise measurements of metabolites (e.g., glucose and lactate) and electrolytes (e.g., sodium and potassium ions)⁹¹ (Fig. 8b). These types of devices provide a real-time assessment of the physiological state of each individual, thereby enabling personalized medicine. As an illustrative demonstration, a wearable patch for sweat-based diabetes monitoring and feedback therapy can thermally actuate polymeric microneedles to deliver Metformin and reduce blood glucose levels in diabetic mice⁹² (Fig. 8c). In another effort to resemble the innate cardiac tissue and confer cardiac conduction system function, electrically conductive epicardial mesh can detect electrical signals reliably and provide electrical stimulation over the ventricles for improved systolic function⁹³ (Fig. 8d).

The idea of deformable structure also enables novel devices to address previously challenging problems such as for high-density, multiplexed neural recording. Being less invasive to the skull limits the size of recording device. Syringe-injectable electronics exploit a crumpled device in a meshed structure dispersed in a solution.⁹⁴ After injected into the brain cavity by a needle, the device would unfold to monitor the local field potentials in different regions of brain. In addition, a soft neural implant or electronic dura mater that embeds interconnects, electrodes, and chemotrodes is capable of extracting cortical states in freely behaving animals and delivering electrochemical spinal neuromodulation to restore locomotion for animals with spinal cord injury⁹⁵ (Fig. 8e). Wireless optogenetic modulation of the spinal cord and peripheral nervous

system has also been demonstrated by integrating radio frequency-powered LEDs in a fully implantable and stretchable system to activate light-sensitive proteins⁹⁶ (Fig. 8f).

With an inspiration from arthropod eyes, digital cameras consisting of a large array of imaging elements on a hemispherical shape (Fig. 8g) have been demonstrated with merits of a wide-angle field of view, low aberrations, high acuity to motion, and an infinite depth of field.⁹⁷ In such array, each element is composed of a soft lens, a Si photodetector, a black matrix, and a black support (Fig. 8g, lower right). Initially fabricated on a flexible, planar geometry, the array is transformed from a hemispherical shape through hydraulic actuation. Continuous change of the curvature of the hemispherical supporting substrate provides a dynamic tuning of the focal plane.⁹⁸

The deformable concept also goes far beyond electronics to soft robots. In an attempt to mimic the function of muscles, soft materials and particularly hydrogels are widely used due to their large deformation and response to external environmental cues. With a combined trigger of temperature and pH value, a micro-robot can manipulate objects repeatedly.⁹⁹ Integrating simple microfluidic networks in the design¹⁰⁰ further enables multiple functions in the soft machine, such as actuation, camouflage, display, temperature regulation, and many more (Fig. 8h). The recent development in soft robotics opens up opportunities from robotic exoskeletons to skeletal muscle replacements and rehabilitation.

FUTURE PERSPECTIVES AND CONCLUSIONS

Future perspectives

As FETs are indispensable components in integrated circuits, integration of emerging low dimensional nanomaterials in FETs provides a unique platform to engineer their electrical and optical properties, with applications from sensors and filters to flexible electronics and advanced optoelectronics. However, continuum theory is no longer valid particularly for low dimensional nanomaterials. Multiscale modeling is then needed to elucidate the coupling among mechanical, electrical, optical, thermal, and even chemical properties in the functional systems and devices. Although being capable of deformation represents another important direction to the current efforts to miniaturize integrated circuits, it is still desirable to integrate high-density electronics to improve their performance while minimizing the footprint.

Conclusions

The review first highlights several stretchable materials and strategies to construct reconfigurable structures. The reconfigurable concept has been applied to low dimensional materials and metamaterials to induce changes in multiple physical properties, including acoustic, electrical, optical, and thermal. The reconfiguration can be introduced by mechanical, thermal, electric, or magnetic trigger, through soft polymers and particularly responsive hydrogels. Integrating various functional components, such as sensors, actuators, communication modules, and power sources, in a single system enables applications from bio-integrated electronics to human-computer interfaces and soft robotics.

ACKNOWLEDGEMENTS

The work is supported by the start-up fund provided by the Engineering Science and Mechanics Department, College of Engineering, and Materials Research Institute at The Pennsylvania State University. The authors also acknowledge the support from NSFC (Grant Nos. 11572161 and 11272260), ASME Haythornthwaite Foundation Research Initiation Grant, and Dorothy Quiggle Career Development Professorship in Engineering at Penn State.

AUTHOR CONTRIBUTIONS

M.D. wrote the section "1D nanomaterials". J.Z. wrote the rest and assembled the figures. H.C. led the preparation of the manuscript and contributed to editorial modifications of the overall text.

ADDITIONAL INFORMATION

Competing interests: The authors declare that they have no competing financial interests.

Publisher's note: Springer Nature remains neutral with regard to jurisdictional claims in published maps and institutional affiliations.

REFERENCES

1. Schaller, R. R. Moore's law: past, present and future. *IEEE Spectrum* **34**, 52–59 (1997).
2. Dresselhaus, M. S. et al. New directions for low-dimensional thermoelectric materials. *Adv. Mater.* **19**, 1043–1053 (2007).
3. Chang, H.-Y. et al. High-performance, highly bendable MoS₂ transistors with high-k dielectrics for flexible low-power systems. *ACS Nano* **7**, 5446–5452 (2013).
4. Kang, P., Wang, M. C., Knapp, P. M. & Nam, S. Crumpled Graphene Photodetector with Enhanced, Strain-Tunable, and Wavelength-Selective Photoresponsivity. *Adv. Mater.* **28**, 4639–4645 (2016).
5. Engheta, N. & Ziolkowski, R. W. *Metamaterials: Physics and Engineering Explorations*. (John Wiley & Sons, 2006).
6. Yang, Z., Dai, H., Chan, N., Ma, G. & Sheng, P. Acoustic metamaterial panels for sound attenuation in the 50–1000 Hz regime. *Appl. Phys. Lett.* **96**, 041906 (2010).
7. Landy, N., Sajuyigbe, S., Mock, J., Smith, D. & Padilla, W. Perfect metamaterial absorber. *Phys. Rev. Lett.* **100**, 207402 (2008).
8. Zhu, J. et al. A holey-structured metamaterial for acoustic deep-subwavelength imaging. *Nat. Phys.* **7**, 52–55 (2011).
9. Cummer, S. A. & Schurig, D. One path to acoustic cloaking. *New J. Phys.* **9**, 45 (2007).
10. Gao, Y. & Cheng, H. Assembly of heterogeneous materials for biology and electronics: from bio-inspiration to bio-integration. *J. Electron Packag.* **139**, 020801 (2017).
11. Rogers, J. A., Someya, T. & Huang, Y. Materials and mechanics for stretchable electronics. *Science* **327**, 1603–1607 (2010).
12. Kim, P., Zarzar, L. D., He, X., Grinthal, A. & Aizenberg, J. Hydrogel-actuated integrated responsive systems (HAIRS): Moving towards adaptive materials. *Curr. Opin. Solid State Mater. Sci.* **15**, 236–245 (2011).
13. Romasanta, L. J., Lopez-Manchado, M. & Verdejo, R. Increasing the performance of dielectric elastomer actuators: A review from the materials perspective. *Prog. Polym. Sci.* **51**, 188–211 (2015).
14. Sekitani, T. & Someya, T. Stretchable, Large-area Organic Electronics. *Adv. Mater.* **22**, 2228–2246 (2010).
15. Yao, S. & Zhu, Y. Nanomaterial-enabled stretchable conductors: strategies, materials and devices. *Adv. Mater.* **27**, 1480–1511 (2015).
16. Cheng, H. & Yi, N. Dissolvable tattoo sensors: from science fiction to a viable technology. *Phys. Scr.* **92**, 013001 (2017).
17. Pelrine, R., Kornbluh, R. & Kofod, G. High-Strain Actuator Materials Based on Dielectric Elastomers. *Adv. Mater.* **12**, 1223–1225 (2000).
18. Lehmann, W. et al. Giant lateral electrostriction in ferroelectric liquid-crystalline elastomers. *Nature* **410**, 447–450 (2001).
19. Oh, J. Y. et al. Intrinsically stretchable and healable semiconducting polymer for organic transistors. *Nature* **539**, 411–415 (2016).
20. Xu, J. et al. Highly stretchable polymer semiconductor films through the nanoconfinement effect. *Science* **355**, 59–64 (2017).
21. Sekitani, T. et al. A rubberlike stretchable active matrix using elastic conductors. *Science* **321**, 1468–1472 (2008).
22. Sun, Y. G., Choi, W. M., Jiang, H. Q., Huang, Y. G. Y. & Rogers, J. A. Controlled buckling of semiconductor nanoribbons for stretchable electronics. *Nat. Nanotechnol.* **1**, 201–207 (2006).
23. Cheng, H., Zhang, Y., Hwang, K.-C., Rogers, J. A. & Huang, Y. Buckling of a stiff thin film on a pre-strained bi-layer substrate. *Int. J. Solids Struct.* **51**, 3113–3118 (2014).
24. Kim, D. H. et al. Materials and noncoplanar mesh designs for integrated circuits with linear elastic responses to extreme mechanical deformations. *Proc. Natl. Acad. Sci. USA* **105**, 18675–18680 (2008).
25. Xu, S. et al. Stretchable batteries with self-similar serpentine interconnects and integrated wireless recharging systems. *Nat. Commun.* **4**, 1543 (2013).
26. Liu, Z., Cheng, H. & Wu, J. Mechanics of solar module on structured substrates. *J. Appl. Mech.* **81**, 064502 (2014).

27. Cheng, H. et al. An analytical model of strain isolation for stretchable and flexible electronics. *Appl. Phys. Lett.* **98**, 061902 (2011).
28. Jang, K.-I. et al. Soft network composite materials with deterministic and bio-inspired designs. *Nat. Commun.* **6**, 6566 (2015).
29. Ma, Q. et al. A nonlinear mechanics model of bio-inspired hierarchical lattice materials consisting of horseshoe microstructures. *J. Mech. Phys. Solids* **90**, 179–202 (2016).
30. Xu, S. et al. Assembly of micro/nanomaterials into complex, three-dimensional architectures by compressive buckling. *Science* **347**, 154–159 (2015).
31. Castellanos-Gomez, A. et al. Local strain engineering in atomically thin MoS₂. *Nano. Lett.* **13**, 5361–5366 (2013).
32. Song, J., Zhou, J. & Wang, Z. L. Piezoelectric and semiconducting coupled power generating process of a single ZnO belt/wire. A technology for harvesting electricity from the environment. *Nano. Lett.* **6**, 1656–1662 (2006).
33. Carlson, A., Bowen, A. M., Huang, Y., Nuzzo, R. G. & Rogers, J. A. Transfer printing techniques for materials assembly and micro/nanodevice fabrication. *Adv. Mater.* **24**, 5284–5318 (2012).
34. Yang, S. Y. et al. Elastomer surfaces with directionally dependent adhesion strength and their use in transfer printing with continuous roll-to-roll applications. *Adv. Mater.* **24**, 2117–2122 (2012).
35. Bachtold, A., Hadley, P., Nakanishi, T. & Dekker, C. Logic circuits with carbon nanotube transistors. *Science* **294**, 1317–1320 (2001).
36. Kocabas, C., Kang, S. J., Ozel, T., Shim, M. & Rogers, J. A. Improved synthesis of aligned arrays of single-walled carbon nanotubes and their implementation in thin film type transistors. *J. Phys. Chem. C* **111**, 17879–17886 (2007).
37. Sangwan, V. K. et al. Fundamental performance limits of carbon nanotube thin-film transistors achieved using hybrid molecular dielectrics. *ACS Nano* **6**, 7480–7488 (2012).
38. Yu, W. J. et al. Adaptive logic circuits with doping-free ambipolar carbon nanotube transistors. *Nano Lett.* **9**, 1401–1405 (2009).
39. Lee, C., Wei, X., Kysar, J. W. & Hone, J. Measurement of the elastic properties and intrinsic strength of monolayer graphene. *Science* **321**, 385–388 (2008).
40. Bertolazzi, S., Brivio, J. & Kis, A. Stretching and breaking of ultrathin MoS₂. *ACS Nano* **5**, 9703–9709 (2011).
41. Tang, D. M. et al. Nanomechanical cleavage of molybdenum disulphide atomic layers. *Nat. Commun.* **5**, 3631 (2014).
42. Tomori, H. et al. Introducing nonuniform strain to graphene using dielectric nanopillars. *Appl. Phys. Express* **4**, 075102 (2011).
43. Qi, J. et al. Piezoelectric effect in chemical vapour deposition-grown atomic-monolayer triangular molybdenum disulfide piezotronics. *Nat. Commun.* **6**, 7430 (2015).
44. Chen, L. et al. Strain-gated field effect transistor of a MoS₂–ZnO 2D–1D hybrid structure. *ACS Nano* **10**, 1546–1551 (2015).
45. Guinea, F., Katsnelson, M. & Geim, A. Energy gaps and a zero-field quantum Hall effect in graphene by strain engineering. *Nat. Phys.* **6**, 30–33 (2010).
46. Bles, M. K. et al. Graphene kirigami. *Nature* **524**, 204–207 (2015).
47. Zhu, S. & Li, T. Hydrogenation-assisted graphene origami and its application in programmable molecular mass uptake, storage, and release. *ACS Nano* **8**, 2864–2872 (2014).
48. Cheng, H. et al. One single graphene oxide film for responsive actuation. *ACS Nano* **10**, 9529–9535 (2016).
49. Lim, H., Jung, J., Ruoff, R. S. & Kim, Y. Structurally driven one-dimensional electron confinement in sub-5-nm graphene nanowrinkles. *Nat. Commun.* **6**, 8601 (2015).
50. Zheludev, N. I. & Plum, E. Reconfigurable nanomechanical photonic metamaterials. *Nat. Nanotechnol.* **11**, 16–22 (2016).
51. Tao, H. et al. Reconfigurable terahertz metamaterials. *Phys. Rev. Lett.* **103**, 147401 (2009).
52. Cheng, W., Wang, J., Jonas, U., Fytas, G. & Stefanou, N. Observation and tuning of hypersonic bandgaps in colloidal crystals. *Nat. Mater.* **5**, 830–836 (2006).
53. Raney, J. R. et al. Stable propagation of mechanical signals in soft media using stored elastic energy. *Proc. Natl. Acad. Sci.* **2016**, 04838 (2016).
54. Li, J. & Chan, C. Double-negative acoustic metamaterial. *Phys. Rev. E* **70**, 055602 (2004).
55. Chen, H. & Chan, C. Acoustic cloaking in three dimensions using acoustic metamaterials. *Appl. Phys. Lett.* **91**, 183518 (2007).
56. Lu, D. & Liu, Z. Hyperlenses and metalenses for far-field super-resolution imaging. *Nat. Commun.* **3**, 1205 (2012).
57. Babae, S., Viard, N., Wang, P., Fang, N. X. & Bertoldi, K. Harnessing deformation to switch on and off the propagation of sound. *Adv. Mater.* **28**, 1631–1635 (2016).
58. Wang, P., Casadei, F., Shan, S., Weaver, J. C. & Bertoldi, K. Harnessing buckling to design tunable locally resonant acoustic metamaterials. *Phys. Rev. Lett.* **113**, 014301 (2014).
59. Rudykh, S. & Boyce, M. C. Transforming wave propagation in layered media via instability-induced interfacial wrinkling. *Phys. Rev. Lett.* **112**, 034301 (2014).
60. Pendry, J. B., Schurig, D. & Smith, D. R. Controlling electromagnetic fields. *Science* **312**, 1780–1782 (2006).
61. Zhu, W. M. et al. Switchable magnetic metamaterials using micromachining processes. *Adv. Mater.* **23**, 1792–1796 (2011).
62. Lee, S. et al. Reversibly stretchable and tunable terahertz metamaterials with wrinkled layouts. *Adv. Mater.* **24**, 3491–3497 (2012).
63. Zarate, Y. et al. Elastic metamaterials for tuning circular polarization of electromagnetic waves. *Sci. Rep.* **6**, 28273 (2016).
64. Cui, Y. et al. Plasmonic and metamaterial structures as electromagnetic absorbers. *Laser Photonics Rev.* **8**, 495–520 (2014).
65. Gansel, J. K. et al. Gold helix photonic metamaterial as broadband circular polarizer. *Science* **325**, 1513–1515 (2009).
66. Kamali, S. M., Arbabi, A., Arbabi, E., Horie, Y. & Faraon, A. Decoupling optical function and geometrical form using conformal flexible dielectric metasurfaces. *Nat. Commun.* **7**, 11618 (2016).
67. Liu, Y. & Zhang, X. Metamaterials: a new frontier of science and technology. *Chem. Soc. Rev.* **40**, 2494–2507 (2011).
68. Halas, N. J., Lal, S., Chang, W.-S., Link, S. & Nordlander, P. Plasmons in strongly coupled metallic nanostructures. *Chem. Rev.* **111**, 3913–3961 (2011).
69. Dong, Z.-G. et al. Plasmonically induced transparent magnetic resonance in a metallic metamaterial composed of asymmetric double bars. *Optics Exp.* **18**, 18229–18234 (2010).
70. Jain, P. K., Huang, W. & El-Sayed, M. A. On the universal scaling behavior of the distance decay of plasmon coupling in metal nanoparticle pairs: a plasmon ruler equation. *Nano Lett.* **7**, 2080–2088 (2007).
71. Zhang, X., Zhang, J., Liu, H., Su, X. & Wang, L. Soft plasmons with stretchable spectroscopic response based on thermally patterned gold nanoparticles. *Sci. Rep.* **4**, 4182 (2014).
72. Ou, J.-Y., Plum, E., Jiang, L. & Zheludev, N. I. Reconfigurable photonic metamaterials. *Nano Lett.* **11**, 2142–2144 (2011).
73. Lee, K. et al. Origami solar-tracking concentrator array for planar photovoltaics. *ACS Photonics* **3**, 2134–2140 (2016).
74. Yang, L. et al. Solution-processed flexible polymer solar cells with silver nanowire electrodes. *ACS Appl. Mater. Interface* **3**, 4075–4084 (2011).
75. Kim, J. et al. Epidermal electronics with advanced capabilities in near-field communication. *Small* **11**, 906–912 (2015).
76. Wang, J. G. et al. Highly flexible graphene/Mn₃O₄ nanocomposite membrane as advanced anodes for Li-ion batteries. *ACS Nano* **10**, 6227–6234 (2016).
77. Wang, G., Zhang, L. & Zhang, J. A review of electrode materials for electrochemical supercapacitors. *Chem. Soc. Rev.* **41**, 797–828 (2012).
78. Peng, L. et al. Ultrathin two-dimensional MnO₂/graphene hybrid nanostructures for high-performance, flexible planar supercapacitors. *Nano Lett.* **13**, 2151–2157 (2013).
79. Pushparaj, V. L. et al. Flexible energy storage devices based on nanocomposite paper. *Proc. Natl. Acad. Sci.* **104**, 13574–13577 (2007).
80. Song, L., Myers, A. C., Adams, J. J. & Zhu, Y. Stretchable and reversibly deformable radio frequency antennas based on silver nanowires. *ACS Appl. Mater. Interface* **6**, 4248–4253 (2014).
81. Li, X. et al. Large-area ultrathin graphene films by single-step marangoni self-assembly for highly sensitive strain sensing application. *Adv. Funct. Mater.* **26**, 1322–1329 (2016).
82. Xu, L. et al. 3D multifunctional integumentary membranes for spatiotemporal cardiac measurements and stimulation across the entire epicardium. *Nat. Commun.* **5**, 3329 (2014).
83. Ying, M. et al. Silicon nanomembranes for fingertip electronics. *Nanotechnology* **23**, 344004 (2012).
84. Jeong, J. W. et al. Materials and optimized designs for human-machine interfaces via epidermal electronics. *Adv. Mater.* **25**, 6839–6846 (2013).
85. Kim, R. H. et al. Stretchable, transparent graphene interconnects for arrays of microscale inorganic light emitting diodes on rubber substrates. *Nano Lett.* **11**, 3381–3886 (2011).
86. Webb, R. C. et al. Ultrathin conformal devices for precise and continuous thermal characterization of human skin. *Nat. Mater.* **12**, 938–944 (2013).
87. Huang, X. et al. Materials and designs for wireless epidermal sensors of hydration and strain. *Adv. Funct. Mater.* **24**, 3846–3854 (2014).
88. Jeong, J. W. et al. Capacitive epidermal electronics for electrically safe, long-term electrophysiological measurements. *Adv. Healthc. Mater.* **3**, 642–648 (2014).
89. Jang, K. I. et al. Rugged and breathable forms of stretchable electronics with adherent composite substrates for transcutaneous monitoring. *Nat. Commun.* **5**, 4779 (2014).
90. Kim, D. H. et al. Epidermal electronics. *Science* **333**, 838–843 (2011).
91. Gao, W. et al. Fully integrated wearable sensor arrays for multiplexed in situ perspiration analysis. *Nature* **529**, 509–514 (2016).
92. Lee, H. et al. A graphene-based electrochemical device with thermoresponsive microneedles for diabetes monitoring and therapy. *Nat. Nanotechnol.* (2016).
93. Park, J. et al. Electromechanical cardioplasty using a wrapped elasto-conductive epicardial mesh. *Sci. Transl. Med.* **8**, 344ra386 (2016).

94. Liu, J. et al. Syringe-injectable electronics. *Nat. Nanotechnol.* **10**, 629–636 (2015).
95. Mineev, I. R. et al. Electronic dura mater for long-term multimodal neural interfaces. *Science* **347**, 159–163 (2015).
96. Park, S. I. et al. Soft, stretchable, fully implantable miniaturized optoelectronic systems for wireless optogenetics. *Nat. Biotechnol.* **33**, 1280–1286 (2015).
97. Song, Y. M. et al. Digital cameras with designs inspired by the arthropod eye. *Nature* **497**, 95–99 (2013).
98. Jung, I. W. et al. Dynamically tunable hemispherical electronic eye camera system with adjustable zoom capability. *Proc. Natl. Acad. Sci. U. S. A* **108**, 1788–1793 (2011).
99. Yoon, C. et al. Functional stimuli responsive hydrogel devices by self-folding. *Smart Mater. Struct.* **23**, 094008 (2014).
100. Morin, S. A. et al. Camouflage and display for soft machines. *Science* **337**, 828–832 (2012).



Open Access This article is licensed under a Creative Commons Attribution 4.0 International License, which permits use, sharing, adaptation, distribution and reproduction in any medium or format, as long as you give appropriate credit to the original author(s) and the source, provide a link to the Creative Commons license, and indicate if changes were made. The images or other third party material in this article are included in the article's Creative Commons license, unless indicated otherwise in a credit line to the material. If material is not included in the article's Creative Commons license and your intended use is not permitted by statutory regulation or exceeds the permitted use, you will need to obtain permission directly from the copyright holder. To view a copy of this license, visit <http://creativecommons.org/licenses/by/4.0/>.

© The Author(s) 2017